HHS Public Access

Author manuscript

J Am Chem Soc. Author manuscript; available in PMC 2021 December 23.

Published in final edited form as:

J Am Chem Soc. 2020 December 23; 142(51): 21243–21248. doi:10.1021/jacs.0c09379.

Valence Dependent Electrical Conductivity in a 3D Tetrahydroxyquinone Based Metal–Organic Framework

Gan Chen[1], **Leland B. Gee**[2], **Wenqian Xu**[3], **Yanbing Zhu**[4], **Juan S. Lezama-Pacheco**[5], **Zhehao Huang**[6], **Zongqi Li**[1], **Jeffrey T. Babicz Jr.**[2], **Snehashis Choudhury**[7], **Ting-Hsiang Chang**[7], **Evan Reed**[1], **Edward I. Solomon**[2,8], **Zhenan Bao**[7,*]

[1]Department of Materials Science and Engineering, Stanford University, Stanford, CA 94305, USA

[2]Department of Chemistry, Stanford University, Stanford, CA 94305, USA

[3]X-ray Science Division, Advanced Photon Source, Argonne National Laboratory, Lemont, IL 60439, USA

[4]Department of Applied Physics, Stanford University, Stanford, CA 94305, USA

[5]Department of Earth System Science, Stanford University, Stanford, CA 94305, USA

[6]Berzelii Centre EXSELENT on Porous Materials, Department of Materials and Environmental Chemistry, Stockholm University, SE-106 91 Stockholm, Sweden

[7]Department of Chemical Engineering, Stanford University, Stanford, CA 94305, USA

[8]Stanford Synchrotron Radiation Lightsource, SLAC National Accelerator Laboratory, Stanford University, Menlo Park, California 94025, USA

Abstract

Electrically conductive metal–organic frameworks (cMOFs) have become a topic of intense interest in recent years due to their great potential in electrochemical energy storage, electrocatalysis and sensing applications. Hitherto most reported cMOFs are 2D structures and 3D cMOFs remain rare. Herein we report a 3D cMOF, namely FeTHQ, synthesized from tetrahydroxy-1,4-quinone (THQ) and Fe(II) sulfate salt. FeTHQ exhibited a conductivity of 3.3 ± 0.55 mS cm^{-1} at 300 K, which is high for 3D cMOFs. The conductivity for FeTHQ is valence dependent. A higher conductivity was measured with the as-prepared FeTHQ than both the air-oxidized and the sodium naphthalenide-reduced sample.

The recent developments of electrically conductive metal-organic frameworks (cMOFs)[1] have significantly increased the range of applications of MOFs in several areas, including energy storage,[2] electrocatalysis,[3] sensors[4] and others.[5] Many works, in the past, have

*Corresponding Author: zbao@stanford.edu.

Author Contributions

The manuscript was written through contributions of all authors.

Supporting Information.

Crystallographic information file for FeTHQ (CCDC-2025662)

The authors declare no competing financial interest

focused on expanding the library of electrically conductive MOFs, yet the majority of these reported cMOFs are layered 2D structures. Extended π-d conjugation over the organic linker and coordination units is often pursued to enable long-range electron delocalization and conductivity in cMOFs and this delocalization is facilitated by the square planar metal sites, thus making 2D cMOFs the most frequently adopted geometry in this class of materials. However, layered 2D structures can have limited surface area and unexposed metal sites due to the stacking of 2D layers. On the contrary, 3D structures may offer 3D porosity and better accessibility.[3e] Currently, 3D cMOFs[3e,5a,6] remain rare species in the literature. Hence, developing new platforms for 3D cMOFs will not only enrich the library of c-MOFs, but also provide exciting opportunities for next-generation applications of conductive MOF materials. Herein, we successfully prepared a 3D cMOF (hereafter referred to as FeTHQ), using octahedral FeO_6 coordination between Fe and the ligand, tetrahydroxy-1,4-quinone (THQ). Furthermore, high conductivity (3.3 ± 0.55 mS cm^{-1} at 300 K) is observed for this 3D cMOF. Since both Fe and the THQ ligand have more than one valence state, the main conduction mechanism for FeTHQ is hypothesized to be redox hopping, which is the origin of high conductivities in several mixed valence 3D MOFs.[5a,7]

FeTHQ was prepared by a solvothermal synthesis at 80 °C, using dimethylformamide (DMF) and water as the co-solvent (Figure 1a; Supporting Information Methods). Specifically, Iron (II) sulfate and THQ were reacted to form the dark navy powders. Recently, another solvothermal synthesis of FeTHQ was demonstrated using water and diethylene glycol as co-solvent at 120°C.[8] The structure model for FeTHQ was obtained from powder X-ray diffraction (PXRD) data and refined by Rietveld refinement (Figure 2a, Figure S1, Table S1) and the final structure (Figure 1b–e) has a cubic unit cell with axis length of 10.5457(2) Å and a space group of $Pm\bar{3}$. For each unit cell (Figure 1c–e), the chemical formula for the main framework is determined to be $Fe_8(C_6O_6)_6$, where C_6O_6 stands for the deprotonated THQ ligand. Slightly different from the recently reported 3D M-THQ structure,[8] the counter cations in the pores are not identified in our structure. As a result, Fe content is obviously lower in our system (Table S2). In our reported CIF, two oxygen sites with large atomic displacement parameters, Ow1 and Ow2 (Figure S2a), which are omitted for simplicity in Figure 1, represent the diffusive electron density of solvent molecules located in the pores (Figure S2). Extended X-Ray absorption fine structure (EXAFS) was used to confirm the local coordination of FeTHQ. The fitted EXAFS (Figure 2b, Figure S4, Table S3) from our structural model agrees very well with the experimental data, thus confirming the validity of our structure model.

Scanning electron microscope (SEM) images (Figure 2c) and transmission electron microscope (TEM) images (Figure S5) show that FeTHQ particles have spherical morphology with the diameter ranging from 150 nm to over 1 μm with substantial interparticle growth. The N_2 adsorption isotherm of FeTHQ degassed at 100 °C (Figure 2d, Figure S6) shows a BET surface area of ~163 m^2 g^{-1} and the pore size distribution matches the crystal structure (Figure S7). The relative low BET surface area is likely caused by the severe interparticle growth which would limit access to the pores and high content of absorbed solvent molecules in the pores.

With the crystal structure confirmed, the electronic structure and electrical properties of FeTHQ were further investigated. Density-functional theory (DFT) calculations were carried out to understand the band structure of this 3D MOF. The band-structure calculations were performed using the projected augmented wave (PAW) method[9] as implemented in the Vienna Ab Initio Simulation Package (VASP)[10] with further information available in Supporting Information (Methods). The results indicate that the majority of bands located near the Fermi energy is contributed by the Fe and O atoms with a non-vanishing density of states at the Fermi level. Visualization of the charge density distribution reveals localization of charge around the molecular framework with limited extension towards the porous vacuum space. Although DFT calculations often underestimate the bandgap for many materials, the simulated band structure and density of states suggest FeTHQ should be conductive with a small bandgap, or gapless.

UV-vis-NIR diffuse reflectance spectroscopy on FeTHQ gave an estimated bandgap of 0.79 eV (Figure 4a). The highest occupied molecular orbital (HOMO) level of 5.23 eV was obtained by photoemission spectroscopy in air (PESA; Figure 4b). Additionally, the conductivity of FeTHQ was measured on pressed pellets (crystallinity preserved during pressing, Figure S8) by four-point probe method. The value exhibits a positive temperature coefficient with an activation energy of 270 meV in the range of 240 to 340 K and a smaller activation energy of 150 meV from 200 to 240 K. The relatively large activation energy is ascribed to the thermally-activated hopping progress at grain boundaries, which dominates the temperature dependence of conductivity in the bulk polycrystalline pellets.[5a,5d,7,11] At 300 K, FeTHQ exhibited an averaged conductivity of 3.3 ± 0.55 mS cm^{-1} (Figure 5a). This conductivity is quite remarkable in comparison to the reported conductivities of other 3D cMOFs, most of which are in the range of 10^{-6} to 1 S cm^{-1}.[5a,6] This example of using nonplanar coordination geometry to enable 3D long range electron transport in framework structures has meaningful implications for designing other 3D conductive MOFs using transition metals adopting nonplanar coordination geometries such as octahedral, tetrahedral, or even more complicated transition metal clusters.

Interestingly, the conductivity of FeTHQ decreased when exposed to ambient air over modest timescales. As shown in Figure 5a, within the same batch of sample, FeTHQ_ox (FeTHQ being exposed to air for 2 weeks) showed a much lower conductivity than the as-prepared FeTHQ. The averaged conductivity dropped from 3.3 ± 0.55 mS cm^{-1} to 0.66 ± 0.059 mS cm^{-1}, showing a five-fold decrease. PXRD (Figure S9) shows that the diffraction pattern of FeTHQ was unchanged in the two weeks, indicating structural change is not playing an important role in the conductivity change. Since the oxidation state of Fe is expected to have great influence on the electronic properties of the MOF, X-ray photoelectron spectroscopy (XPS) and ^{57}Fe Mössbauer spectroscopy were utilized to examine the oxidative state of Fe.

High resolution XPS of Fe (Figure S10a) for FeTHQ displayed a rather broad $2p_{3/2}$ peak at ~710.0 eV, which falls between the range of Fe^{2+} (FeO ~709.5 eV) and Fe^{3+} (Fe_2O_3 ~711 eV) oxides[12] and could be indicative of mixed valence Fe in the MOF. To confirm this, ^{57}Fe Mössbauer spectroscopy was carried out. The Mössbauer spectrum for FeTHQ at 80 K (Figure 5b) is composed of at least three species. The dominant species (68.2%, Table S4)

has an isomer shift of 0.54 mm/s and quadrupole splitting of 0.95 mm/s. These values combined with the observed magnetic hyperfine splitting in the 6 K Mössbauer spectrum (Figure S11) align with a ferric species,[13] with the isomer shift and relatively low quadrupole splitting consistent with a S=5/2 high-spin ferric Fe site. The second fitted species (28.5%, Table S4) has an isomer shift of 1.10 mm/s and quadrupole splitting of 2.45 mm/s, consistent with an S=2 high-spin ferrous species.[13] Another minor ferrous peak (3.3%) is also observed. The Mössbauer spectrum of the filtrate control sample (Figure S12), e.g. excess Fe in the solvothermal synthesis, indicate that the species observed in the MOF are not unreacted ferrous sulfate precursor species in the solvent. Assuming that there are no other counter ions in the as prepared framework, THQ ligand is calculated to carry 3.56 negative charges on average instead of 4 from charge neutrality, suggesting that THQ also exhibits mixed valence characteristics. Therefore, FeTHQ is identified to be a dual mixed valence system.

After air oxidation, the Fe $2p_{3/2}$ XPS spectra (Figure S10a) shifted slightly towards higher binding energy, exhibiting a peak at 710.5 eV. This suggests that Fe in the MOF turned to higher oxidation state during the air exposure process. Again, ^{57}Fe Mössbauer spectroscopy was used to analyze the composition of Fe in FeTHQ_ox sample (Figure 5c). The Mössbauer spectrum for FeTHQ_ox is also fitted by three species. The dominant species with ferric parameters is 85.9% of the spectrum and the two ferrous species together are only 14.1% (Table S4). It appears that the ferrous component is converted to the ferric component in the presence of oxygen. Air oxidation lead to an even more unbalanced Fe^{3+}/Fe^{2+} ratio, which makes the redox hopping less likely to happen and leads to a drop in the mobility of electrons. In addition, FeTHQ was recently reported to exhibit n-type behavior,[8] suggesting electrons are the majority carriers in this framework. The oxidation would result in a drop of electron density in the framework. These two factors together may have caused the large drop in conductivity. While the conversion of ferrous Fe to ferric Fe is concomitant with a loss in conductivity, subtle electronic changes in the coordination environment around Fe may have contributed to this conductivity change as well. The minor differences in C1s and O1s XPS (Figure S10) between the as prepared and air oxidized FeTHQ samples indicate that the ligand is also somewhat oxidized during the oxidation.

Since redox hopping is essential for FeTHQ's high conductivity, higher conductivity can be realized with a more balanced Fe^{3+}/Fe^{2+} ratio. FeTHQ was reduced with sodium naphthalenide (Figure 5a,d; Supporting Information Methods).[14] PXRD on the reduced samples showed no obvious structural change for the framework in the reduction process (Figure S13). In the most reduced sample, "FeTHQ_red4", the ferric species is 42.8 % of the spectrum and the ferrous species is 57.2 % (Figure 5d, Table S4). Surprisingly, the conductivity of FeTHQ decreases with reduction (Figure 5a), although a more balanced Fe^{3+}/Fe^{2+} ratio is achieved. The reason for the conductivity drop is likely due to the heterogenous nature of the reduction reaction (FeTHQ solid reacting with sodium naphthalenide solution) and FeTHQ's limited pore volume and surface area. Fe sites within the particles are less accessible to reduction and the surface layer of each FeTHQ particle would get reduced first and more easily. This heterogenous reduction produced a highly reduced surface layer for FeTHQ particles, which lacks in spatial distribution the balance between different valence states and therefore does not facilitate redox hopping. These

reduction studies and the reduction of FeTHQ_ox (Figure S14, 15) provide proof that redox hopping is the primary conduction mechanism for FeTHQ and a balance between different valence states that have an even intraparticle distribution is desired for high conductivity.

In this work, we presented a mixed valence cMOF, FeTHQ, with high electrical conductivity in the cubic 3D framework. Its conductivity is found to be sensitive to valence change. The high conductivity from FeTHQ demonstrates that square planar conjugation is not mandatory for achieving efficient long-range charge transport and it is possible to build 3D conductive MOFs through nonplanar coordination geometries. With high conductivity and rich redox chemistry (Figure S16), FeTHQ may demonstrate potential in electrochemical applications such as supercapacitors and batteries. The relevant studies are under way.

Supplementary Material

Refer to Web version on PubMed Central for supplementary material.

ACKNOWLEDGMENT

We acknowledge support from US Department of Energy, Office Basic Energy Sciences, Division of Material Science and Engineering, Program on Physical Behaviors of Materials (DE-SC0016523). Part of this work was performed at the Stanford Nano Shared Facilities (SNSF), supported by the National Science Foundation under award ECCS-1542152. Use of the Stanford Synchrotron Radiation Lightsource, SLAC National Accelerator Laboratory, is supported by the U.S. Department of Energy, Office of Science, Office of Basic Energy Sciences under Contract No. DE-AC02-76SF00515. This research used resources of the Advanced Photon Source, a U.S. Department of Energy (DOE) Office of Science User Facility operated for the DOE Office of Science by Argonne National Laboratory under Contract No. DE-AC02-06CH11357. This research was also partially supported by the National Institute of Health R01GM040392 (E.I.S.) and F32GM122194 (L.B.G.). Z.H. acknowledges the support from the Swedish Research Council (VR, 2016-04625).

REFERENCES

(1). (a)Sun L; Campbell MG; Dincă M Electrically Conductive Porous Metal-Organic Frameworks. Angew. Chem. Int. Ed 2016, 55 (11), 3566–3579.(b)Ko M; Mendecki L; Mirica KA Conductive Two-Dimensional Metal-Organic Frameworks as Multifunctional Materials. Chem. Commun 2018, 54 (57), 7873–7891.(c)Hmadeh M; Lu Z; Liu Z; Gándara F; Furukawa H; Wan S; Augustyn V; Chang R; Liao L; Zhou F; Perre E; Ozolins V; Suenaga K; Duan X; Dunn B; Yamamto Y; Terasaki O; Yaghi OM New Porous Crystals of Extended Metal-Catecholates. Chem. Mater 2012, 24 (18), 3511–3513.(d)Kambe T; Sakamoto R; Hoshiko K; Takada K; Miyachi M; Ryu J-H; Sasaki S; Kim J; Nakazato K; Takata M; Nishihara H Π-Conjugated Nickel Bis(Dithiolene) Complex Nanosheet. J. Am. Chem. Soc 2013, 135 (7), 2462–2465. [PubMed: 23360513]

(2). (a)Sheberla D; Bachman JC; Elias JS; Sun C-J; Shao-Horn Y; Dincă M Conductive Mof Electrodes for Stable Supercapacitors with High Areal Capacitance. Nat. Mater 2017, 16 (2), 220–224. [PubMed: 27723738] (b)Feng D; Lei T; Lukatskaya MR; Park J; Huang Z; Lee M; Shaw L; Chen S; Yakovenko AA; Kulkarni A; Xiao J; Fredrickson K; Tok JB; Zou X; Cui Y; Bao Z Robust and Conductive Two-Dimensional Metal-Organic Frameworks with Exceptionally High Volumetric and Areal Capacitance. Nature Energy 2018, 3 (1), 30–36.(c)Li W-H; Ding K; Tian H-R; Yao M-S; Nath B; Deng W-H; Wang Y; Xu G Conductive Metal-Organic Framework Nanowire Array Electrodes for High-Performance Solid-State Supercapacitors. Adv. Funct. Mater 2017, 27 (27), 1702067.(d)Park J; Lee M; Feng D; Huang Z; Hinckley AC; Yakovenko A; Zou X; Cui Y; Bao Z Stabilization of Hexaaminobenzene in a 2d Conductive Metal-Organic Framework for High Power Sodium Storage. J. Am. Chem. Soc 2018, 140 (32), 10315–10323. [PubMed: 30041519] (e)Wang F; Liu Z; Yang C; Zhong H; Nam G; Zhang P; Dong R; Wu Y; Cho J; Zhang J; Feng X Fully Conjugated Phthalocyanine Copper Metal–Organic Frameworks for Sodium–Iodine Batteries with Long-Time-Cycling Durability. Adv. Mater 2020, 32 (4),

1905361.(f)Cai D; Lu M; Li L; Cao J; Chen D; Tu H; Li J; Han W A Highly Conductive Mof of Graphene Analogue Ni3(Hitp)2 as a Sulfur Host for High-Performance Lithium–Sulfur Batteries. Small 2019, 15 (44), 1902605.

(3). (a)Miner EM; Fukushima T; Sheberla D; Sun L; Surendranath Y; Dincă M Electrochemical Oxygen Reduction Catalysed by Ni3(Hexaiminotriphenylene)2. Nat. Commun 2016, 7 (1), 10942. [PubMed: 26952523] (b)Miner EM; Wang L; Dincă M Modular O2 Electroreduction Activity in Triphenylene-Based Metal-Organic Frameworks. Chem. Sci 2018, 9 (29), 6286–6291. [PubMed: 30123483] (c)Clough AJ; Yoo JW; Mecklenburg MH; Marinescu SC Two-Dimensional Metal–Organic Surfaces for Efficient Hydrogen Evolution from Water. J. Am. Chem. Soc 2015, 137 (1), 118–121. [PubMed: 25525864] (d)Downes CA; Clough AJ; Chen K; Yoo JW; Marinescu SC Evaluation of the H2 Evolving Activity of Benzenehexathiolate Coordination Frameworks and the Effect of Film Thickness on H2 Production. ACS Appl. Mat. Interfaces 2018, 10 (2), 1719–1727.(e)Matheu R; Gutierrez-Puebla E; Monge MÁ; Diercks CS; Kang J; Prévot MS; Pei X; Hanikel N; Zhang B; Yang P; Yaghi OM Three-Dimensional Phthalocyanine Metal-Catecholates for High Electrochemical Carbon Dioxide Reduction. J. Am. Chem. Soc 2019, 141 (43), 17081–17085. [PubMed: 31613614] (f)Zhong H; Ghorbani-Asl M; Ly KH; Zhang J; Ge J; Wang M; Liao Z; Makarov D; Zschech E; Brunner E; Weidinger IM; Zhang J; Krasheninnikov AV; Kaskel S; Dong R; Feng X Synergistic Electroreduction of Carbon Dioxide to Carbon Monoxide on Bimetallic Layered Conjugated Metal-Organic Frameworks. Nat. Commun 2020, 11 (1), 1409. [PubMed: 32179738] (g)Zhong H; Ly KH; Wang M; Krupskaya Y; Han X; Zhang J; Zhang J; Kataev V; Büchner B; Weidinger IM; Kaskel S; Liu P; Chen M; Dong R; Feng X A Phthalocyanine-Based Layered Two-Dimensional Conjugated Metal-Organic Framework as a Highly Efficient Electrocatalyst for the Oxygen Reduction Reaction. Angew. Chem. Int. Ed 2019, 58 (31), 10677–10682.(h)Lian Y; Yang W; Zhang C; Sun H; Deng Z; Xu W; Song L; Ouyang Z; Wang Z; Guo J; Peng Y Unpaired 3d Electrons on Atomically Dispersed Cobalt Centres in Coordination Polymers Regulate Both Oxygen Reduction Reaction (Orr) Activity and Selectivity for Use in Zinc–Air Batteries. Angew. Chem. Int. Ed 2020, 59 (1), 286–294.(i)Jia H; Yao Y; Zhao J; Gao Y; Luo Z; Du P A Novel Two-Dimensional Nickel Phthalocyanine-Based Metal–Organic Framework for Highly Efficient Water Oxidation Catalysis. J. Mater. Chem. A 2018, 6 (3), 1188–1195.

(4). (a)Campbell MG; Liu SF; Swager TM; Dincă M Chemiresistive Sensor Arrays from Conductive 2d Metal-Organic Frameworks. J. Am. Chem. Soc 2015, 137 (43), 13780–13783. [PubMed: 26456526] (b)Campbell MG; Sheberla D; Liu SF; Swager TM; Dincă M Cu3(Hexaiminotriphenylene)2: An Electrically Conductive 2d Metal-Organic Framework for Chemiresistive Sensing. Angew. Chem. Int. Ed 2015, 54 (14), 4349–4352.(c)Yao M-S; Lv X-J; Fu Z-H; Li W-H; Deng W-H; Wu G-D; Xu G Layer-by-Layer Assembled Conductive Metal-Organic Framework Nanofilms for Room-Temperature Chemiresistive Sensing. Angew. Chem. Int. Ed 2017, 56 (52), 16510–16514.(d)Ko M; Mendecki L; Eagleton AM; Durbin CG; Stolz RM; Meng Z; Mirica KA Employing Conductive Metal-Organic Frameworks for Voltammetric Detection of Neurochemicals. J. Am. Chem. Soc 2020, 142 (27), 11717–11733. [PubMed: 32155057]

(5). (a)Darago LE; Aubrey ML; Yu CJ; Gonzalez MI; Long JR Electronic Conductivity, Ferrimagnetic Ordering, and Reductive Insertion Mediated by Organic Mixed-Valence in a Ferric Semiquinoid Metal-Organic Framework. J. Am. Chem. Soc 2015, 137 (50), 15703–15711. [PubMed: 26573183] (b)DeGayner JA; Jeon I-R; Sun L; Dincă M; Harris TD 2d Conductive Iron-Quinoid Magnets Ordering up to Tc = 105 K Via Heterogenous Redox Chemistry. J. Am. Chem. Soc 2017, 139 (11), 4175–4184. [PubMed: 28230984] (c)Jeon I-R; Negru B; Van Duyne RP; Harris TDA 2d Semiquinone Radical-Containing Microporous Magnet with Solvent-Induced Switching from Tc = 26 to 80 K. J. Am. Chem. Soc 2015, 137 (50), 15699–15702. [PubMed: 26573055] (d)Yang C; Dong R; Wang M; Petkov PS; Zhang Z; Wang M; Han P; Ballabio M; Bräuninger SA; Liao Z; Zhang J; Schwotzer F; Zschech E; Klauss H-H; Cánovas E; Kaskel S; Bonn M; Zhou S; Heine T; Feng X A Semiconducting Layered Metal-Organic Framework Magnet. Nat. Commun 2019, 10 (1), 3260. [PubMed: 31332187] (e)Huang X; Zhang S; Liu L; Yu L; Chen G; Xu W; Zhu D Superconductivity in a Copper(Ii)-Based Coordination Polymer with Perfect Kagome Structure. Angew. Chem. Int. Ed 2018, 57 (1), 146–150.(f)Huang X; Sheng P; Tu Z; Zhang F; Wang J; Geng H; Zou Y; Di C.-a.; Yi Y; Sun Y; Xu W; Zhu D A Two-Dimensional Π–D Conjugated Coordination Polymer with Extremely High Electrical Conductivity and

Ambipolar Transport Behaviour. Nat. Commun 2015, 6 (1), 7408. [PubMed: 26074272] (g)Arora H; Dong R; Venanzi T; Zscharschuch J; Schneider H; Helm M; Feng X; Cánovas E; Erbe A Demonstration of a Broadband Photodetector Based on a Two-Dimensional Metal-Organic Framework. Adv. Mater 2020, 32 (9), 1907063.(h)Lahiri N; Lotfizadeh N; Tsuchikawa R; Deshpande VV; Louie J Hexaaminobenzene as a Building Block for a Family of 2d Coordination Polymers. J. Am. Chem. Soc 2017, 139 (1), 19–22. [PubMed: 27936659] (i)Sun L; Liao B; Sheberla D; Kraemer D; Zhou J; Stach EA; Zakharov D; Stavila V; Talin AA; Ge Y; Allendorf MD; Chen G; Léonard F; Dincă M A Microporous and Naturally Nanostructured Thermoelectric Metal-Organic Framework with Ultralow Thermal Conductivity. Joule 2017, 1 (1), 168–177.

(6). (a)Aubrey ML; Wiers BM; Andrews SC; Sakurai T; Reyes-Lillo SE; Hamed SM; Yu C-J; Darago LE; Mason JA; Baeg J-O; Grandjean F; Long GJ; Seki S; Neaton JB; Yang P; Long JR Electron Delocalization and Charge Mobility as a Function of Reduction in a Metal-Organic Framework. Nat. Mater 2018, 17 (7), 625–632. [PubMed: 29867169] (b)Xie LS; Sun L; Wan R; Park SS; DeGayner JA; Hendon CH; Dincă M Tunable Mixed-Valence Doping toward Record Electrical Conductivity in a Three-Dimensional Metal-Organic Framework. J. Am. Chem. Soc 2018, 140 (24), 7411–7414. [PubMed: 29807428] (c)Skorupskii G; Dincă M Electrical Conductivity in a Porous, Cubic Rare-Earth Catecholate. J. Am. Chem. Soc 2020, 142 (15), 6920–6924. [PubMed: 32223159]

(7). (a)Sun L; Hendon CH; Park SS; Tulchinsky Y; Wan R; Wang F; Walsh A; Dincă M Is Iron Unique in Promoting Electrical Conductivity in Mofs? Chem. Sci 2017, 8 (6), 4450–4457. [PubMed: 28616149] (b)Xie LS; Skorupskii G; Dincă M Electrically Conductive Metal–Organic Frameworks. Chem. Rev 2020, 120 (16), 8536–8580. [PubMed: 32275412]

(8). Wu X; Qiu Y; Chen Z; Guan B; Hao X; Rykov AI; Sun Y; Liu L; Zou Y; Sun J; Xu W; Zhu D Paramagnetic Conducting Metal-Organic Frameworks with Three-Dimensional Structure. Angew. Chem. Int. Ed 2020, 59 (47), 20873–20878.

(9). Kresse G; Joubert D From Ultrasoft Pseudopotentials to the Projector Augmented-Wave Method. Phys. Rev. B 1999, 59 (3), 1758–1775.

(10). (a)Kresse G; Furthmüller J Efficient Iterative Schemes for Ab Initio Total-Energy Calculations Using a Plane-Wave Basis Set. Phys. Rev. B 1996, 54 (16), 11169–11186.(b)Blöchl PE Projector Augmented-Wave Method. Phys. Rev. B 1994, 50 (24), 17953–17979.

(11). Dou J-H; Sun L; Ge Y; Li W; Hendon CH; Li J; Gul S; Yano J; Stach EA; Dincă M Signature of Metallic Behavior in the Metal-Organic Frameworks M3(Hexaiminobenzene)2 (M = Ni, Cu). J. Am. Chem. Soc 2017, 139 (39), 13608–13611. [PubMed: 28910095]

(12). Yamashita T; Hayes P Analysis of Xps Spectra of Fe2+ and Fe3+ Ions in Oxide Materials. Appl. Surf. Sci 2008, 254 (8), 2441–2449.

(13). Gütlich P; Bill E; Trautwein AX, Hyperfine Interactions In Mössbauer Spectroscopy and Transition Metal Chemistry: Fundamentals and Applications, Gütlich P; Bill E; Trautwein AX, Eds Springer Berlin Heidelberg: Berlin, Heidelberg, 2011; 73–135.

(14). Connelly NG; Geiger WE Chemical Redox Agents for Organometallic Chemistry. Chem. Rev 1996, 96 (2), 877–910. [PubMed: 11848774]

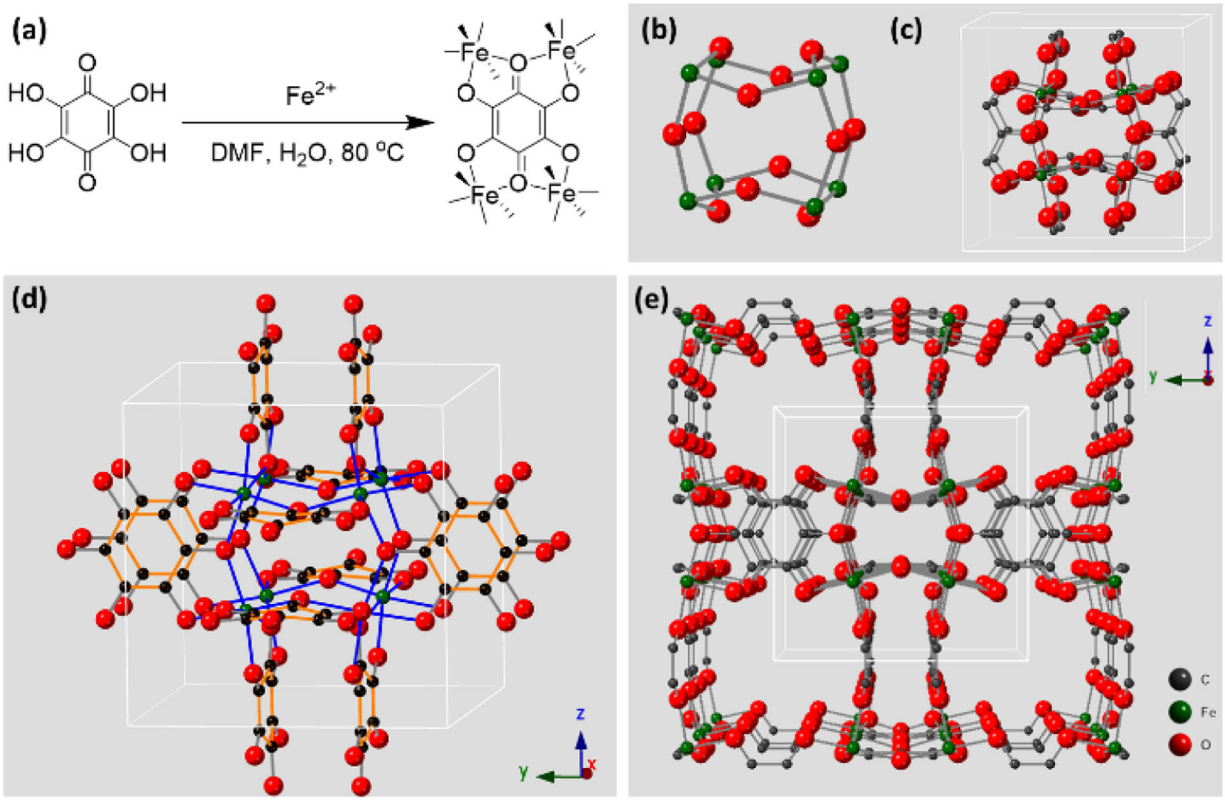

Figure 1.

(a) The synthetic scheme for FeTHQ; (b) the Fe octamer and (c) the unit cell structure of FeTHQ; (d) the unit cell structure of FeTHQ with extended THQ ligand; (e) expanded framework structure for FeTHQ.

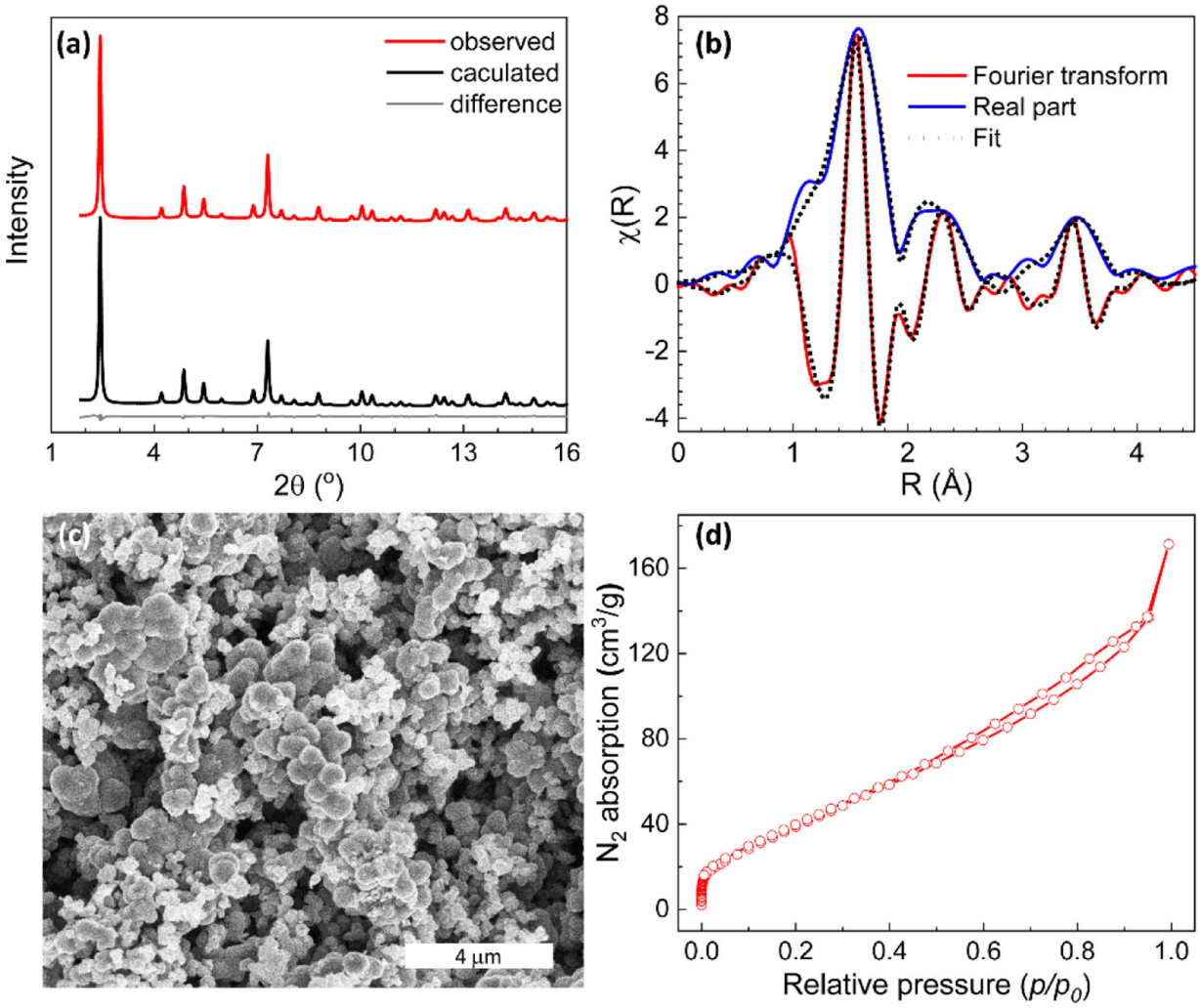

Figure 2.

(a) Rietveld refinement of FeTHQ PXRD displaying the observed pattern (black) (λ = 0.4481 Å), calculated pattern (red), difference plot (gray); (b)The Fourier transform (red) and the magnitude of the real part (blue) for Fe K-edge EXAFS of FeTHQ; (c) SEM of FeTHQ powders; (d) N_2 sorption isotherm of FeTHQ, degassed at 60°C for 2 hours followed by 100°C for 8 hours.

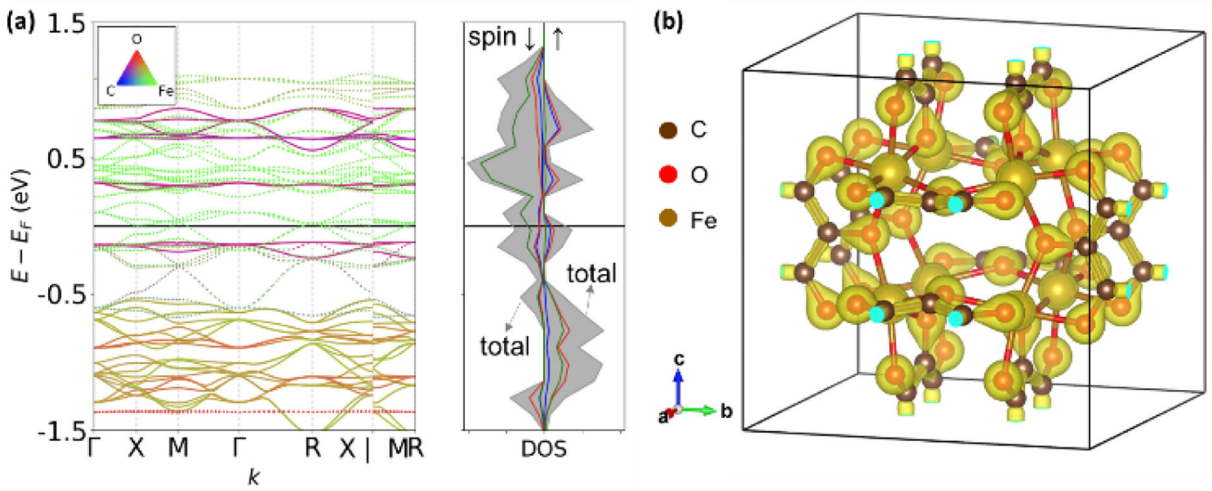

Figure 3.

(a) The band-structure and element-projected density of states and (b) associated charge density distribution of FeTHQ.

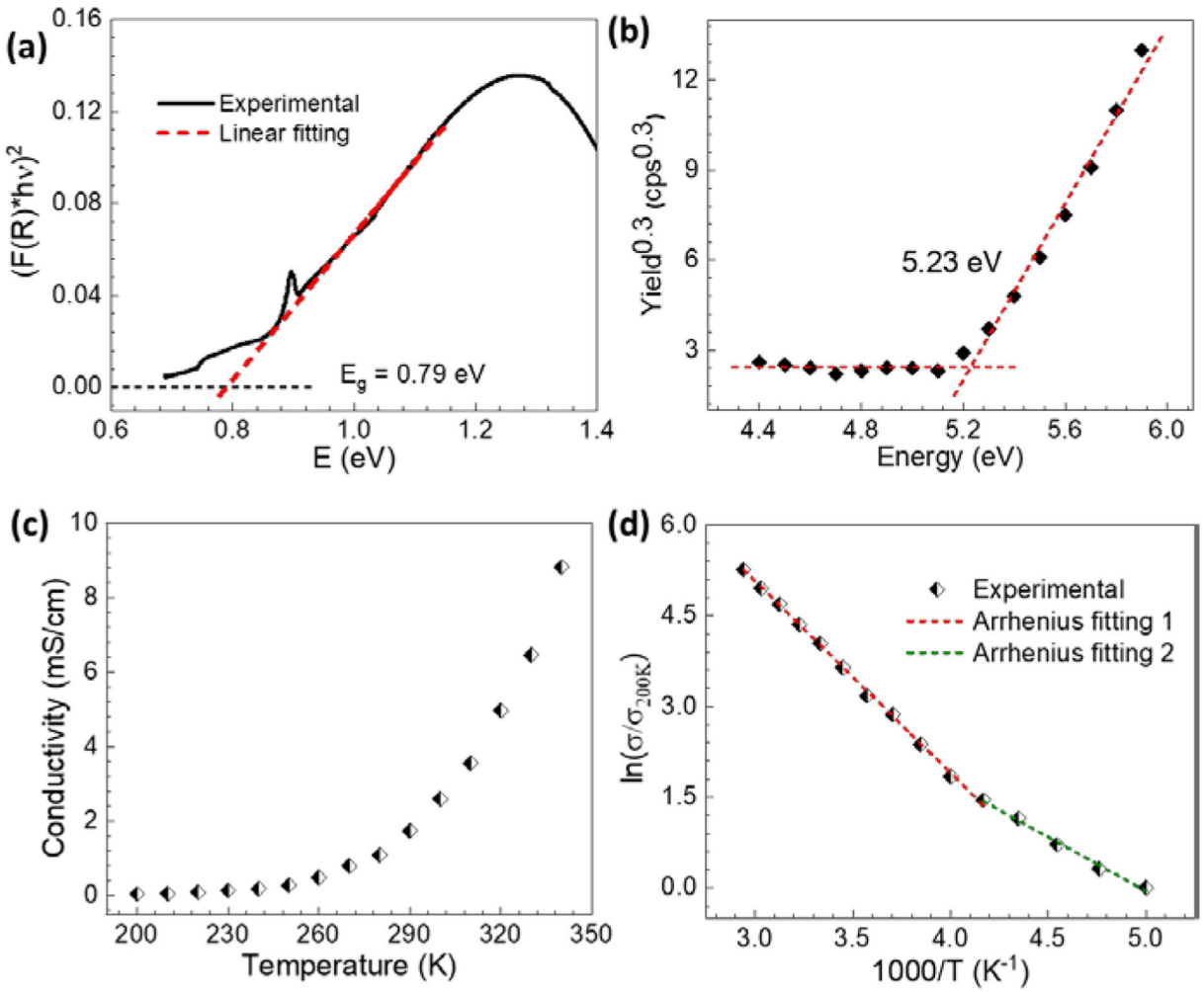

Figure 4.

(a) Tauc plot (black) of a KBr pellet containing 0.25 wt% FeTHQ deduced from the UV–vis–NIR diffuse reflectance spectrum; (b) PESA of FeTHQ; (c) Variable-temperature conductivity for a ~200 μm thick FeTHQ pellet; (d) Arrhenius fitting of temperature dependent conductivity data.

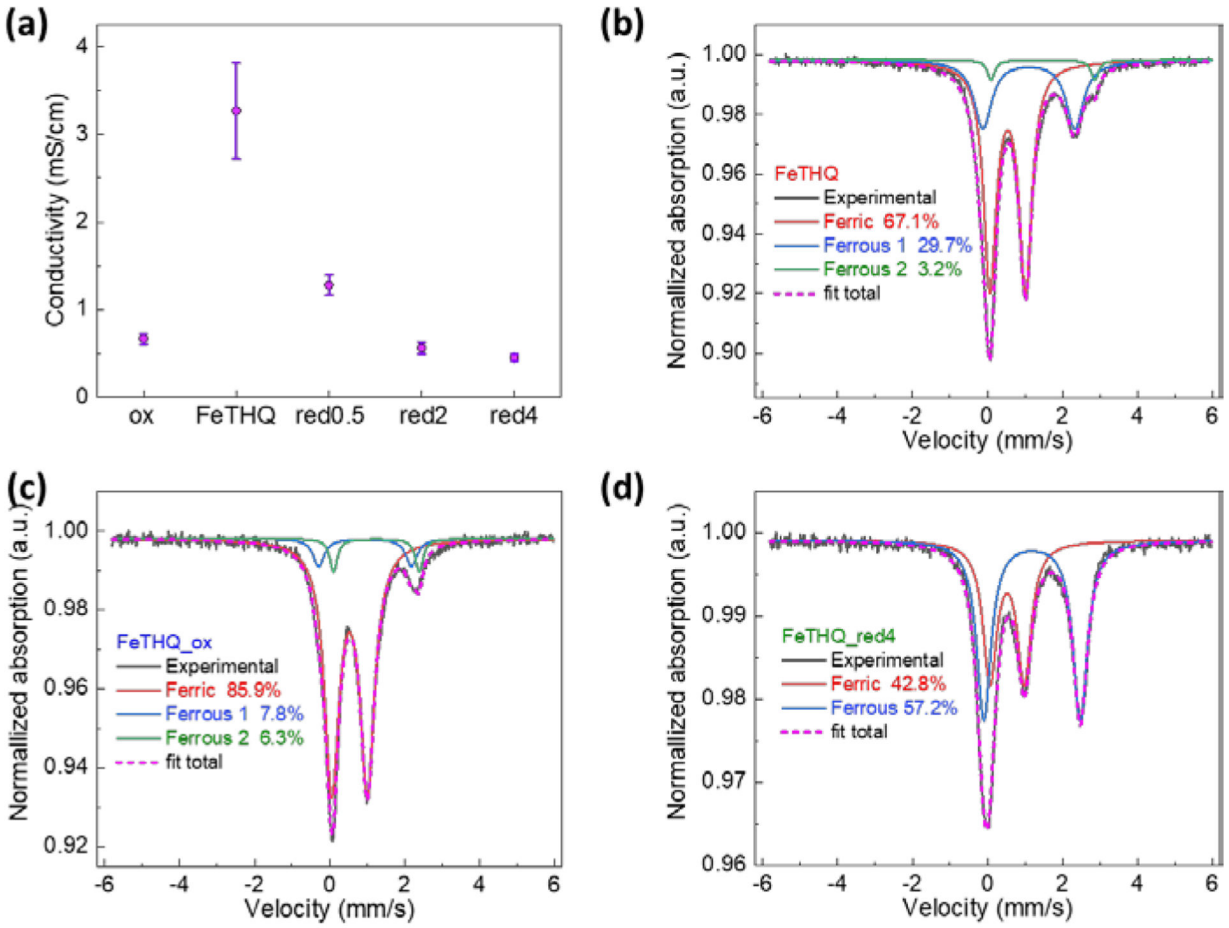

Figure 5.

(a) Conductivity for FeTHQ samples: FeTHQ—as prepared, FeTHQ_ox—FeTHQ air oxidized for two weeks, FeTHQ_red0.5/2/4—100 mg as prepared FeTHQ reduced with 0.5/2/4 ml 0.2 M freshly prepared NaC_8H_{10}; Mössbauer spectroscopy for (b) FeTHQ, (c) FeTHQ_ox and (d) FeTHQ_red4 at 80 K.